SYNTHESIS, SINTERING AND CHARACTERIZATION OF Al_2O_3-13 wt. % TiO_2 COMPOSITE POWDER PREPARED BY POLYMER ASSISTED CO-PRECIPITATION ROUTE

A THESIS SUBMITTED IN PARTIAL FULFILLMENT OF THE REQUIREMENT FOR THE DEGREE OF

MASTER OF TECHNOLOGY

IN

INDUSTRIAL CERAMICS

BY

NEERA SINGH
ROLL NO-212CR2507

DEPARTMENT OF CERAMIC ENGINEERING
NATIONAL INSTITUTE OF TECHNOLOGY
ROURKELA, ORISSA-769008
2013-2014

SYNTHESIS, SINTERING AND CHARACTERIZATION OF Al_2O_3-13 wt. % TiO_2 COMPOSITE POWDER PREPARED BY POLYMER ASSISTED CO-PRECIPITATION ROUTE

A THESIS SUBMITTED IN PARTIAL FULFILLMENT OF THE REQUIREMENT FOR THE DEGREE OF

MASTER OF TECHNOLOGY
IN
INDUSTRIAL CERAMICS

BY

NEERA SINGH
ROLL NO-212CR2507

Under the guidance of
Prof. RANABRATA MAZUMDER

DEPARTMENT OF CERAMIC ENGINEERING
NATIONAL INSTITUTE OF TECHNOLOGY
ROURKELA, ORISSA-769008
2013-2014

National Institute of Technology, Rourkela

CERTIFICATE

This is to certified that the work contained in the project entitled "**Synthesis, sintering and characterization of Al_2O_3-13 wt. % TiO_2 composite powder prepared by polymer assisted co-precipitation route"** submitted by **Neera Singh** (212CR2507) in partial fulfillment of the Project for the award of **Master of Technology** Degree in **Ceramic Engineering** at the National Institute of Technology, Rourkela is an authentic work carried out by her under my supervision and guidance. To the best of my knowledge, the matter embodied in the thesis has not been submitted to any other university / institute for the award of any Degree or Diploma.

Prof. RANABRATA MAZUMDER
DEPARTMENT OF CERAMIC ENGINEERING
NATIONAL INSTITUTE OF TECHNOLOGY
ROURKELA – 769008

ACKNOWLEDGEMENT

I have taken efforts in this project. However, it would not have been possible without the kind support and help of many individuals and our organization **NIT, ROURKELA**. I would like to extend my sincere thanks to all of them.

I am highly indebted to **Prof. RANABRATA MAZUMDAR** for their guidance and constant supervision as well as for providing necessary information regarding the project & also for their support in completing the project. He gave me the golden opportunity to do this wonderful project on the topic Alumina-Titania nano composite which also helped me in doing a lot of research and I came to know about so many new things.

I would like to express my special gratitude and thanks to our **Head of the Department**, **Prof. S.K. PRATIHAR** for giving me such attention and time.

I would like to express my gratitude towards all the faculty members of ceramic department for their kind co-operation and encouragement which help me in completion of this project.

My thanks and appreciations also go to my colleagues in developing the project and people who have willingly helped me out with their abilities.

Neera Singh (212cr2507)

Department of Ceramic Engineering

National Institute of Technology, Rourkela

ABSTRACT

Composites of alumina (Al_2O_3) and titania (TiO_2) are known for their high toughness, low thermal expansion, and low thermal conductivity. Alumina-Titania coatings are excellent candidates for providing protection against abrasive wear, resistant to high temperature erosion with cryogenic compatibility, high adhesion strength, and are resistant to high thermal shock. High temperature formation of Al_2TiO_5 (AT) is reason for the excellent property. It is reported in literature that nano-composite of Al_2O_3-TiO_2 or Al_2O_3-AT has 2-3 times better thermo-mechanical property. In most of the cases Al_2O_3-TiO_2 composite powder prepared by mechanical mixing of nano alumina and titania powder which are costly. There are very few reports on in-situ synthesis of Al_2O_3-TiO_2 composite by simple wet chemical method.

In our present work, an alumina-titania composite powder containing 13 wt.% titania was prepared by polymer assisted co-precipitation technique. Co-polymer Pluronic P-123 was used in the precipitation process. The influence and effect of concentration of the surfactant on the morphology and size of the obtained materials were investigated. The particle size for polymer assisted composite powder is found to be less than the sample prepared by the simple co-precipitation process. The phase evolution and reaction mechanism was studied by XRD and DSC-TG. The Fourier transformation infrared spectroscopy (FTIR) measurement was carried out in order to investigate the presence of polymer. The particle size and morphology was analyzed for with and without polymer synthesized powder. Densification behavior of nano-composite powder was studied by dilatometry. 95% of sintered density can be achieved at 1650^{o}C. Our derived process is able to achieve homogeneous distribution of Al_2O_3-Al_2TiO_5 phase in sintered samples.

CONTENTS

LIST OF TABLES

LIST OF FIGURES

LIST OF ABBREVATIONS

Al	Aluminum
Ti	Titanium
O	Oxygen
H	Hydrogen
H_2SO_4	Sulphuric Acid
HNO_3	Nitric Acid
$TiCl_4$	Titanium tetra chloride
AT	Aluminium Titanate
Al_2TiO_5	Aluminum Titanate
WOP	Sample Without polymer content
15P	Sample having 15 wt. %polymer content
30 P	Sample having 30 wt. %polymer content
100 P	Sample having 100 wt. %polymer content
α	Alpha
γ	Gamma
θ	Theta
SEM	Scanning Electron Microscope

XRD	X – Ray Diffraction
DSC	Differential Scanning Calorimetry
wt.%	Weight percentage
FESEM	Field Emission Scanning Electron Microscope
DLS	Dynamic Light Scattering
FTIR	Foureir Transformation Infrared
TG	Thermogravimetry
DIL	Dilatometry
UTM	Universal Testing Machine
µm	Micrometer
nm	Nanometer
IR	Infrared
cm	Centimeter

Chapter 1

INTRODUCTION

1. INTRODUCTION

Alumina-titania composites are desirable materials for high performance coating applications where thermal barriers are required [1].These are known for their high toughness, low thermal expansion, and low thermal conductivity. They also provide excellent abrasive wear resistance to high temperature erosion with cryogenic compatibility, high adhesion strength, and high thermal shock resistance. Presence of Al_2TiO_5 phase improves the thermomechanical property of composite. It is also reported that Al_2TiO_5 exhibits microcracking during cooling from the sintering temperature especially above the critical sintered grain size of 1.5 μm. That necessiates for obtaining fine-grained microstructures [2]. Metals have a low emissivity over the whole spectrum and thus cannot dissipate heat by radiating in the thermal infrared region. It is well known that most polar bonding oxides show strong efficiency of photon emission thus exhibiting a high emissivity value. Al_2O_3-TiO_2 coating has high thermal emmisivity (>0.95) [3]. Al_2O_3-13wt% TiO_2 composite was most studied due to its better thermomechanical property. It has been found that coatings of Al_2O_3-13wt% TiO_2 nanoparticles have better properties (like higher abrasive wear resistance, twice fracture toughness and good bond strength) than the properties of Metco130 [4]. As there are very few reports on in-situ synthesis of Al_2O_3-TiO_2 composite powder by wet chemical method and also mechanical mixing of nanopowder is very costly so we target to prepare the Al_2O_3-TiO_2 composite by polymer assisted co-precipitation route. We also want to achieve complete conversion of TiO_2 phase to Al_2TiO_5 in sintered product.

Chapter 2

LITERATURE SURVEY

2.1 ALUMINIUM OXIDE (Al_2O_3):

Aluminium oxide has the chemical formula Al_2O_3 and it is a chemical compound of aluminium and oxygen. Most commonly it is identified as aluminium (III) oxide. Commonly it is known as alumina, and also known as aloxite, aloxide and alundum based on their forms and applications. The polymorphic phase alpha alumina has crystalline nature and comprises the mineral corundum which has different precious forms like ruby and sapphire. Al_2O_3 has its application to obtain metal aluminium, as a refractory material owing to its high melting point [5]. Rubies have laser quality by the trace of chromium with deep red color. Impurities like iron and titanium has effect on the colors of sapphire. Al_2O_3 has very high thermal conductivity, electrical insulation and very good abrasive resistance which make it suitable for refractory applications. [5]. It has its applications in different areas such as optics [6], biomedical [7, 8], electronics field [9].

Corundum is the most common form of crystalline aluminium oxide in which hexagonal close-packed structure is formed by nearly oxygen ions and octahedral interstices are filled by aluminium ions. Center of each Al_{3+} is octahedral. There are also other phases of aluminium oxide; those are γ-, δ-, η-, θ-, and χ- Al_2O_3 [10] Each phase can be characterized by its own structure and properties.

Table 1: Properties of Aluminium Oxide (Al_2O_3)

Molecular Formula	Al_2O_3
Appearance	White solid
Density	3.96–4.2 g/cm3
Melting Point	2,072 °C
Boiling point	2,977 °C
Refractive index (*n*D)	nω=1.768–1.772

	nε=1.760–1.763 Birefringence 0.008
Solubility	practically insoluble in ethanol and also insoluble in diethyl ether and water

2.2 TITANIUM DI OXIDE (TiO_2):

TiO_2 is commonly known as titania which is the oxide of titanium. When it has its application in pigment, it is called titanium white. The main source of TiO_2 is ilmenite, rutile and anatase. The main applications of titania is in paint, sunscreen, food coloring etc. Rutile, anatase and brookite are the natural forms of Titanium di oxide. The main source of TiO_2 is ilmenite ore which is the most common form of titanium dioxide-bearing ore. Next most common form is rutile which contains approximately 98%titanium dioxide in the ore. Above the temperature range 600-800^{0}C, the metastable phases anatase and brookite irreversibly converts to the equilibrium rutile phase. [11]

Table 2: Properties of Titanium di Oxide (TiO_2)

Molecular Formula	TiO_2
Appearance	White solid
Density	4.24 g/cm^3 (Rutile) 3.77 g/cm^3 (Anatase)
Melting Point	1844 °C
Boiling point	2973 °C
Refractive index (*n*D)	2.489 (Anatase) 2.584 (Brookite)

	2.608 (Rutile)
Solubility	Insoluble in water

The most common application of titania is in paints, varnishes and plastics, which is about 80% of the total consumption of TiO_2. Remaining 8% includes other applications like cosmetic products, printing inks, rubber, fibers, food materials etc. The other applications are in glass and glass ceramics, solar cell [12], humidity sensors [13], in the production of pure titanium, electrical ceramics, photo catalyst [14] and chemical intermediates [15]

In spite of having various properties and applications, Alumina and titania each has individual shortcomings, For example Alumina has decreased activity and titania has lower surface area with low thermal stability [16, 17]. It is reported that the combination of these two oxides may provide improved characteristic material in which the shortcomings of these oxides can be improved [18]. This type of mixture may enhance the applications available to this material. Aluminium titanate (Al_2TiO_5) is used in materials for aeronautical and automotive purposes [19], in medical applications like orthopedic and dental implants [20], in petroleum hydro treatments [21] and as a potential adsorbent in the decontamination of chemical warfare agents [18].

2.3 ALUMINIUM TITANATE:

Parts of Al_2TiO_5 are difficult to process because they have thermal instability, highly anisotropic structure, and density difference between the constituent oxides. Al_2O_3 has 3.99 g/cm^3, rutile TiO_2 has 4.25 g/cm^3, and final Al_2TiO_5 3.70 g/cm^3.

Aluminum titanate has several interesting properties such as low thermal expansion coefficient, low thermal conductivity, excellent thermal shock resistance, and high melting point. Materials which have low thermal expansion coefficients are in continuous demand to improve thermal efficiency in missiles, electronics, and engines. These following properties fulfill the demands to be used in many advanced applications such as thermal barriers, explosion engine parts, metal smelting, and as support material for catalyst [21, 22].

Structure: Al_2TiO_5 is isomorphous with the structure of pseudo brookite (Fe_2TiO_5) crystallizing in the orthorhombic space group with a = 3.591Å, b = 9.429Å and c = 9.636Å lattice parameters [23]. Six oxygen ions surround each Al_{3+} or Ti_{4+} cation which forms distorted oxygen octahedral in this structure with weak bonds. Structure of this material shows strong thermal anisotropy, results in a localized internal stresses during cooling which causes considerable micro cracking and it is responsible for the decrease in mechanical properties of the material, low thermal expansion and an excellent thermal shock resistance [24]. It has been reported from the papers that a decrease in the grain size helps in minimizing the micro cracking [25, 26].Low thermal expansion and a certain amount of porosity results in the good thermal shock resistance. The good thermal shock resistance is a result of the low thermal expansion and a certain amount of porosity in the microstructure. This property makes this material to withstand the sudden temperature changes without any damage. Aluminium titanate has poor wettability with molten metals which makes it ideal for foundry work and metallurgical smelting applications.

Table 3: Properties of Aluminium Titanate

Property	**Range**
Thermal expansion coefficient	(0.2–1)×10−6 K−1
Thermal conductivity	0.9–1.5Wm−1 K−1

Thermal shock resistance	≈500Wm−1
Melting point	1860 ◦C
Young's modulus	17-20 GPa
Thermal insulation	1.5 W/mK

2.3.1 EQUILIBRIUM PHASE DIAGRAM:

$$Al_2TiO_5 \Leftrightarrow Al_2O_3 + TiO_2$$

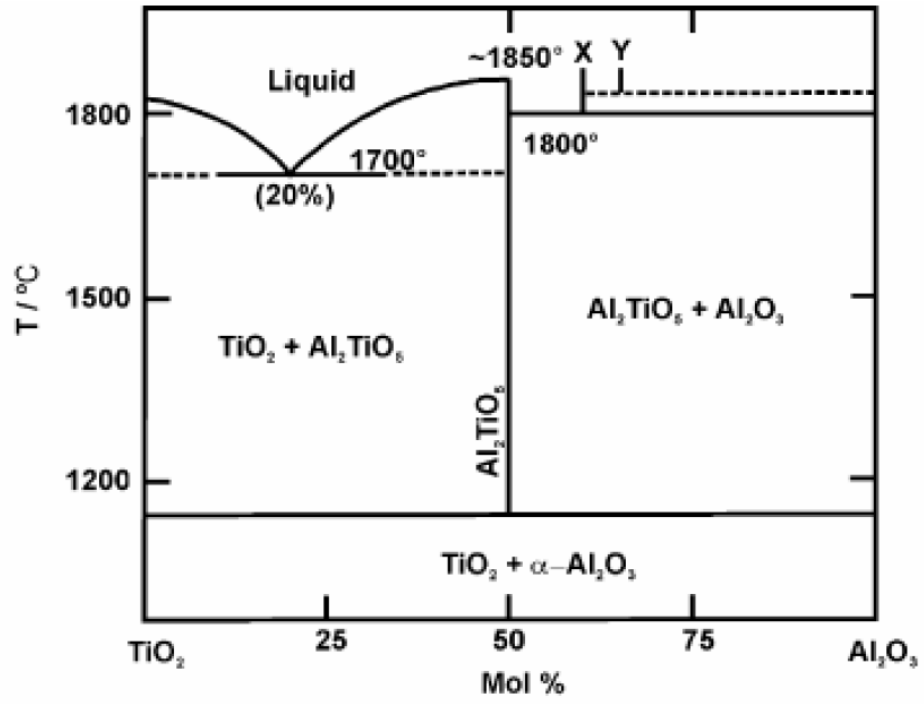

Fig 1: Phase diagram of Al2O3-TiO2 system [27]

Meybodi et al. [28] prepared Al_2O_3–20 wt. %AT composites by the reaction sintering of alumina and titania nano powders at different temperatures. The relative density of the composite after sintering at 1500^{o}C was 94.1%. No further increase in density was detected which is attributed to

agglomeration of particles with in the initial mixture. The XRD pattern analysis confirmed the formation of aluminium titanate in the Al_2O_3–20 wt. % composite sintered at 1300–1500^oC. Elevated sintering temperatures also improved the hardness to 8.5GPa.

Borrell et al. [29] obtained fully dense alumina- 40 vol. % aluminium titanate composites by colloidal filtration and fast reaction-sintering of alumina/titania green bodies by spark plasma sintering at low temperatures (1250–1400^oC). The composites obtained had near-to-theoretical density (>99%) with a bimodal grain size distribution. Phase development analysis demonstrated that aluminium titanate has already formed at 1300^oC. The mechanical properties such as Vickers hardness, flexural strength and fracture toughness of bulk composites are significantly higher than those reported elsewhere, e.g. the composite sintered at 1350^oC show values of about 24 GPa, 424 MPa and 5.4 MPa $m^{1/2}$, respectively. The improved mechanical properties of these composites are attributed to the enhanced densification and the finer and more uniform nanostructure achieved by non-conventional fast sintering of slip-cast dense green compacts.

Jayasankar et al. [30] prepared nano size alumina–aluminium titanate composite through a titania coated alumina particle precursor. They have used $TiCl_4$ as precursor of TiO_2 which is hazardous and costly. The starting alumina particle size has no significant influence on the formation temperature of aluminium titanate in the composite. XRD analysis confirms the formation of aluminium titanate in the Al–20%AT composite sintered at 1350°C and having >98% sintered density. SEM photograph of sintered composite shows that the average grain size of the composite varied with respect to the initial particle size of alumina.

2.4 Preparation of Al_2O_3-TiO_2 composite by different route:

Okamura et al. [31] prepared an unagglomerated, monosized $Al_2O_3TiO_2$ composite powder by the stepwise hydrolysis of titanium alkoxide in an Al_2O_3 dispersion. Particle size was controlled by selecting the particle size of the starting Al_2O_3 powder; TiO_2 content was determined by the amount of alkoxide hydrolyzed. A composite-powder compact containing 50 mol.% TiO_2, when fired at 1350°C for 30 min, showed nearly theoretical density with aluminum titanate phase formation.

Li et al. [32] fabricated Al_2O3–13 wt. %TiO_2 coatings by plasma spraying and laser-remelting on titanium alloys with reconstituted sub-micrometer powders and conventional Metco 130 powders. The microstructural evolution of the coatings during the compound process has been investigated in details. The micrographs of the mechanically mixed Al_2O_3-TiO_2 powders and Metco 130 powders are shown in Fig 2.

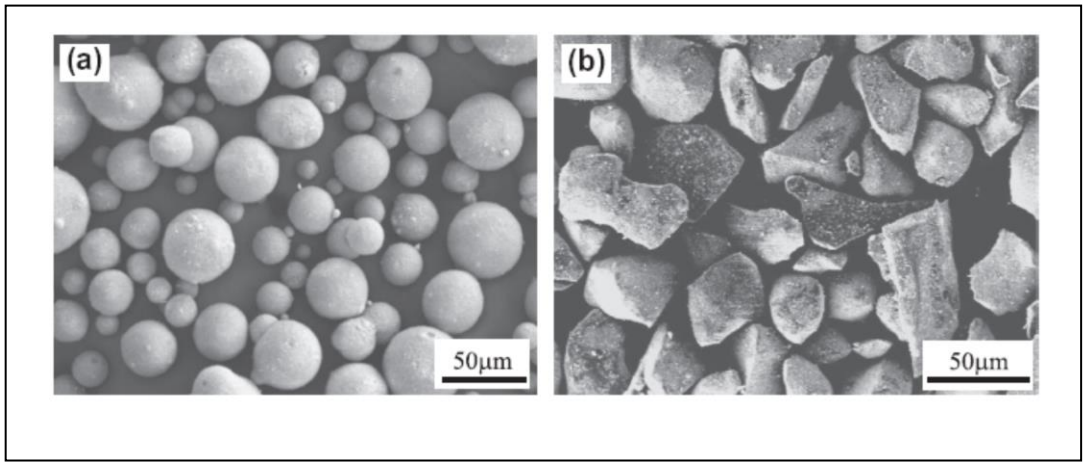

Fig. 2: SEM micrographs of Al_2O_3–13 wt. %TiO_2 powders (a) Mechanically mixed powders, and (b) Metco 130 powders.

2.5 OTHER APPLICATION OF TiO_2-Al_2O_3 NANOCOMPOSITE

Lee et al. [33] synthesized TiO_2-Al_2O_3 nanocomposite **(**Al_2O_3 content 2-50wt%**)** by alkoxide based sol-gel route process, simultaneously gelling aluminum and titanium alkoxide. Focusing on surface phenomena and thermal stability of synthesized nanocomposites, this research describes the way by which alumina binds to the TiO_2 anatase phase and how the new framework modifies the photo physical and surface properties to achieve complete 2,4 Dichlorophenoxiacetic acid (2,4-D) degradation with $t^{1/2}$= 38.3 min^{-1}. Then a nano composite with 5wt% of Al_2O_3 shows optimum textural, adsorption abilities, and photo catalytic properties.

Dashliborun et al. [34] studied gas phase photo catalytic degradation of methyl ethyl ketone (MEK) using nano- TiO_2 supported γ -Al_2O_3 (20-80) adsorbent was studied in a Fluidized Bed Photo-Reactor (FBPR).TiO_2 mediated photo catalytic oxidation process (PCO) is an interesting method for treatment of VOCs in the air stream. In this method, which is based on overcoming the band gap energy of TiO_2 using ultra violet radiation, the electron–hole pairs form in the surface of TiO_2. These pairs participate in reductive and oxidative reactions to form the reactive species such as hydroxyl radicals (OH^-) and superoxide radicals (O_2). These reactive species attack to VOCs molecules and convert them to carbon dioxide and water.

Arier et al. studied [35] the effects of Al_2O_3: TiO_2 ratios on the structural and optical properties of TiO_2–Al_2O_3 nano-composite films which were synthesized by sol–gel method. They used titanium but oxide {Ti (OC_4H_9)$_4$} as Ti-source and studied for different Al_2O_3: TiO_2 volume ratios of 0.025, 0.05, 0.1 and 0.2.Their results indicate that an increase in Al_2O_3: TiO_2volume ratio leads to the increase in the crystal sizes of nanoparticles in TiO_2–Al_2O_3 nano-composite films due to the rising agglomeration. Band gap values of TiO_2–Al_2O_3 nano-composite thin films were also changed by different Al_2O_3: TiO_2 ratios.

Narrow size distribution Al_2O_3- TiO_2 composite powders containing nominally 10 to 60 mol % TiO_2 were prepared by the stepwise hydrolysis of titanium alkoxide in Al_2O_3 dispersion [36]. Particle size was controlled by selecting the particle size of the starting Al_2O_3 powder. The TiO_2 content was determined by the amount of alkoxide hydrolysed. Composite powder compacts were prepared by filter casting or centrifugal casting the composite powder dispersions. All compacts had similar shrinkage behavior during sintering. When fired above 1300°C, the compacts containing less than 50 mol. % TiO_2 became Al_2TiOs-Al_2O_3 composite bodies with high densities, the compact containing 50 mol. % TiO_2 became an Al_2TiOs body with domain structure, and the compact containing 60 mol. % TiO_2 formed a TiO_2-Al_2TiOs composite structure. When these composite bodies were annealed below 1300^oC, they showed different decomposition behavior and microstructures.

2.6 CO-PRECIPITATION ROUTE:

Co-precipitation means carrying down by substance's precipitate which is normally soluble under the employed conditions [37]. In Co precipitation method, joint precipitation is done from the solution of soluble salt which is followed by washing, drying and calcinations. Co-precipitation can be done by two different routes. First is direct precipitation route in which the precipitator is added and mixed homogenously to the salt solution and second is inverse precipitation route in which salt solution is poured and stirred into the precipitator to get precipitate. In second method, the formed precipitate is more finely dispersed than the precipitate by first method [38]. It increases the solid state interaction and accordingly decreases the sintering temperature.

Co precipitation method offers following advantages. They are:

1. Simple and rapid preparation
2. Easy control of particle size and composition
3. Various possibilities to modify the particle surface state and overall homogeneity
4. Smallest size particles with rounded shape can be obtained by using co-precipitation route [39].

2.6.1 EFFECT OF POLYMER ADDITION IN COPRECIPITATION ROUTE:

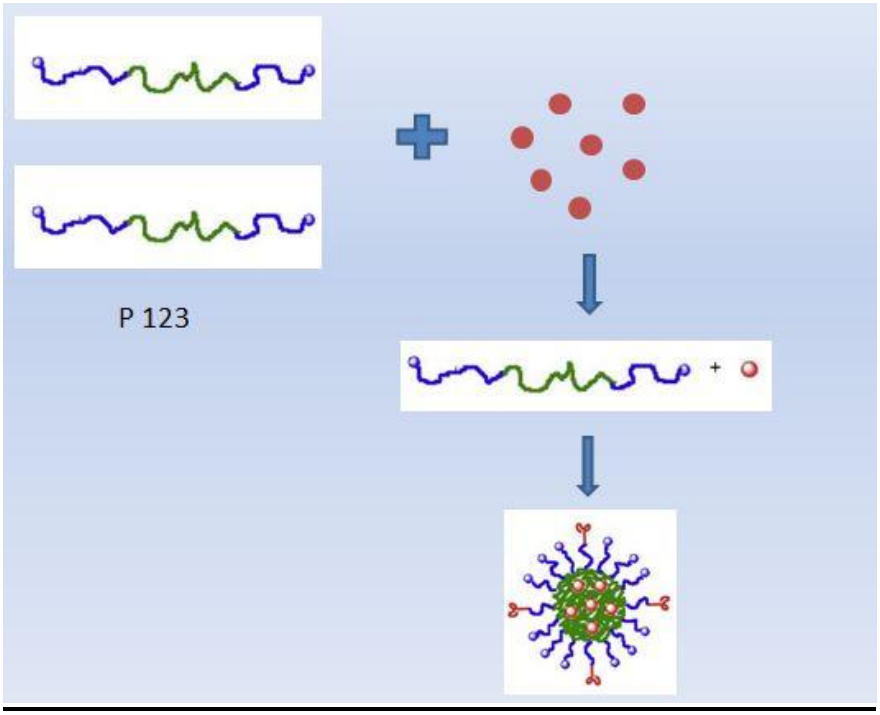

Fig 3: shows the mechanism of polymer with the sample particles showing hydrophobic and hydrophilic nature simultaneously.

Jose'ORTIZ-LANDEROS [40] compared the conventional hydrothermal route with varying the reaction time and temperature and investigated the difference in the particle size and crystallization of BaTiO3. They obtained nano fine grained microstructure with the use of BaTiO3. For the synthesis of Li2SiO3 powder, they used a surfactant named as TRITON X-114 and obtained the microstructure having hollow microspheres.

Yu-Tzu Huang [41] reported the hydroxyapatite synthesis by co-precipitation with the use of a stabilizer triblock co-polymer F127. He reported that in the synthesis of Hydroxyapatite, F127 is acting as a stabilizer inspite of structure directing agent. The use of stabilizer helps in getting uniform nanoparticles as compared to the HA prepared without using any surfactant.

Zeinab Mosayebi [42] reported the effect of surfactant used in co-precipitation route as well as the effect of other parameter such as refluxing temperature, time and calcination temperature in the synthesis of Magnesium aluminate spinel. They successfully synthesized the Nano crystalline Magnesium Aluminate with Nano crystalline size and high surface area. This high surface area was achieved by the addition of pluronic P123 triblock Co-polymer which presents the agglomeration.

Rongrong Jiang [43] investigated the effect of surfactant on the particle size as well as shape of MnO_2 powders prepared by co-precipitation route and stated that the sample prepared with the use of surfactant has all loose clew shapes whereas the particles without surfactant were spherical and larger as compared to earlier powders. He also investigated the maximum concentration of surfactant which can be used to get smaller particle size which was critical Micelle concentration above which the surface area was again reduced.

O.L. Galkina [44] prepared TiO_2 material by using polymer assisted sol gel process and investigated the effect of polymer on the particle size distribution. According to their

investigation, the Rutile content was decreased and Anatase content was increased as 24% and 76% respectively. With the use of surfactant P123 which means that this surfactant retarded the formation of rutile and helps in producing the Anatase Nano crystals with smallest size. Again, an another surfactant's behavior was investigated which was polyethylenimine which increased the rutile phase and decreased anatase phase as 64 and 36% respectively by which crystallite size was increase. It means it has the opposite behavior than Pluronic P123.

OBJECTIVE OF THE THESIS

As there are very few reports on in-situ synthesis of Al_2O_3-TiO_2 composite powder by wet chemical method and also mechanical mixing of nanopowder is very costly so we target to prepare the Al_2O_3-TiO_2 composite by polymer assisted co-precipitation route. We also want to achieve complete conversion of TiO_2 phase to Al_2TiO_5 in sintered product.

Chapter 3

EXPERIMENTAL WORK

3.1 RAW MATERIALS AND PREPARATION OF INITIAL MATERIALS:

The initial chemicals used were Al $(NO_3)_3.9H_2O$ (Merck, GR), titanium nitrate solution, nitric acid, H_2SO_4, Ammonia solution etc. To prepare the titanium nitrate solution, the ammonium sulfate was dissolved in heated H_2SO_4 solution. Titania was completely dissolved in that solution which was cooled to room temperature. This solution was added in the distilled water (1:3 ratio) in a chilled water bath. This solution was well stirred and kept for some time. Ammonia solution was added very slowly while stirring up to pH level 11. Centrifuge washing was done to achieve pH level up to 6-7. Now, HNO_3 was added in distilled water (1:1) and stirred in a chilled water bath. Washed precipitate was dissolved in this solution very slowly without stirring which was finally filtered. After completion of this process TiO_2 estimation was done to check the strength of TiO_2 in solution.

3.2 POLYMER USED AND ITS PROPERTIES:

Two types of polymers in different concentrations were used and then compared with the simple co precipitation route. Co polymer P 123(SIGMA-ALDRICH) is used here. P 123 is known as poly (ethylene glycol) – block – poly (propylene glycol) – block – poly (ethylene glycol) and also known as PEG – PPG – PEG Pluronic P 123. Which is highly viscous and having the chemical formula $(C_3H_6O.C_2H_4O)_X$. This polymer has molecular weight approximately Mn = 5800. Finally the powder prepared by simple co precipitation and polymer assisted (P123) co-precipitation route are characterized to compare their behavior.

FLOW CHART: 1

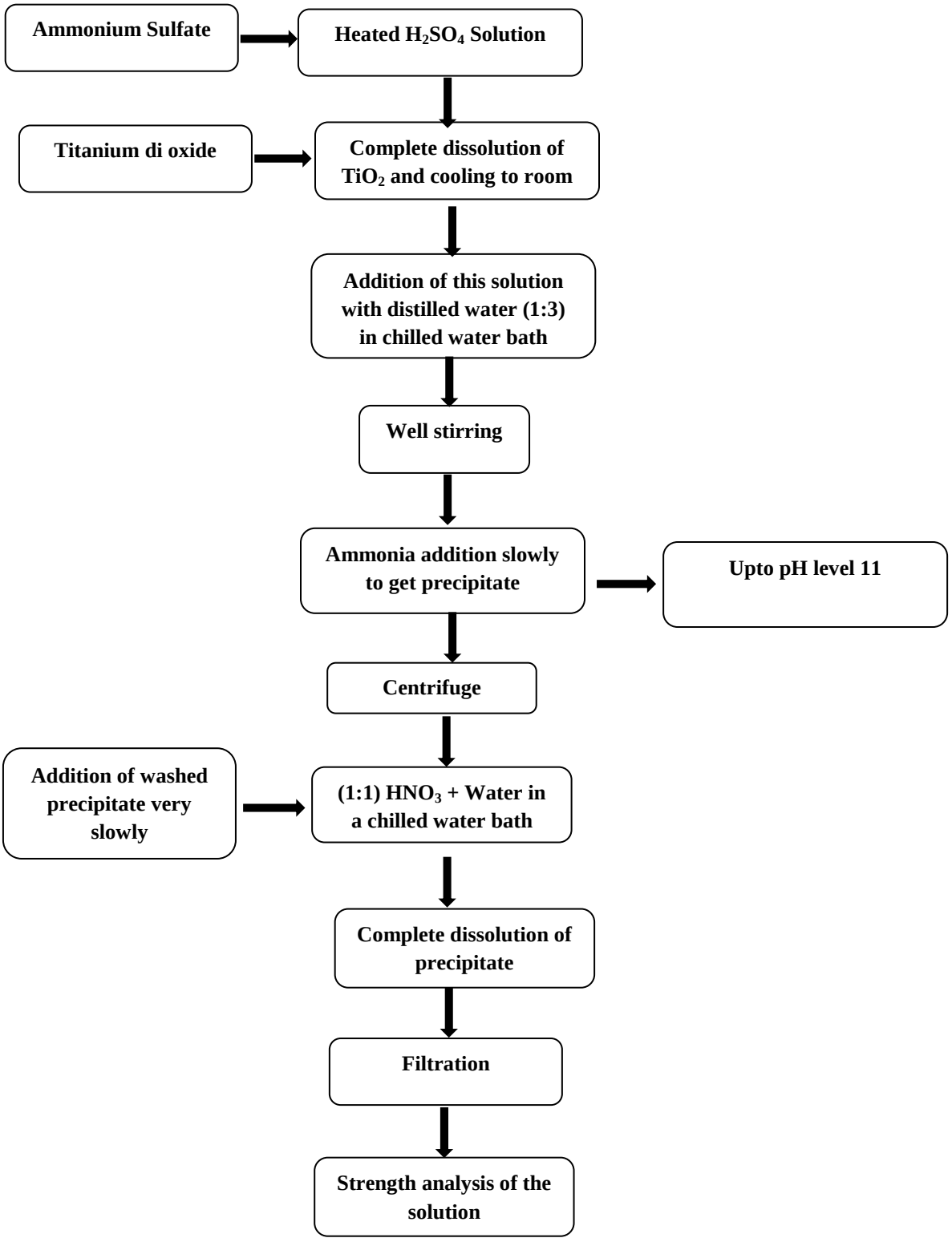

Fig. 4: Flow diagram for the preparation of Titanium-Nitrate solution

3.3 SYNTHESIS:

3.3.1 SIMPLE CO PRECIPITATION ROUTE:

For the synthesis of alumina titania composite, co- precipitation route was used which was then followed by polymer assisted co- precipitation and then results were compared. In simple co-precipitation route, aluminum nitrate solution of 0.5 moles was prepared. Calculated amount of titanium nitrate solution was added as required for 13% TiO_2. This metal nitrate solution was slowly mixed with diluted ammonia solution up to pH level 9-10. Precipitation was formed during this mixing process which cannot be filtered by normal filtration due to the formation of gel like mass. So centrifuge washing was done up to pH level 6-7 to remove the nitrate part. Final washing was done with alcohol. This washed precipitate was dried at 60-70°C for about 1-2 days which is then grinded and calcined at 300^{o}C, 600^{o}C for 6 hr, 1000°C and then 1200°C for 4 hrs. Various techniques such as X-ray diffraction; particle size analysis, differential scanning calorimeter (DSC)/ thermo gravimetric analysis (TGA) and field emission scanning electron microscopy (FESEM) analysis were utilized to characterize the prepared samples.

3.3.2 POLYMER ASSISTED CO-PRECIPITATION ROUTE:

Polymer assisted co-precipitation route can be used to achieve the particles of high surface area. The amount of polymer in polymer assisted co-precipitation route was varied to see the difference in results. The concentration of polymer utilized was 15%, 30% and then 100% wt% of total Al_2O_3 and TiO_2. In this route, calculated amount of polymer was added in the prepared aluminum nitrate solution while heating and stirring. This process was continued till the complete dissolution of polymer to make a homogenous solution. Now the calculated amount of titanium nitrate solution was added to get 13 wt% TiO_2 and stirring is done to make a complete

homogenous solution. This metal nitrate solution is titrated very slowly with diluted ammonia solution for precipitate formation up to pH value of 9-10. This precipitate was centrifuged to remove ammonia up to pH level 6-7. Final washing was done with alcohol. This precipitate was dried at 60-70^{0}C for 1-2 days. After drying it is grinded and calcined at 300^{0}C and 600^{0}C for 6 hrs and then 1000^{0}C followed by 1200^{0}C, both for 4 hours. Again the same characterization techniques were utilized to compare the difference in results. Figure shows the flow chart for synthesis of alumina-titaniana nano composite by simple co-precipitation and polymer assisted co-precipitation route.

FLOW CHART: 2

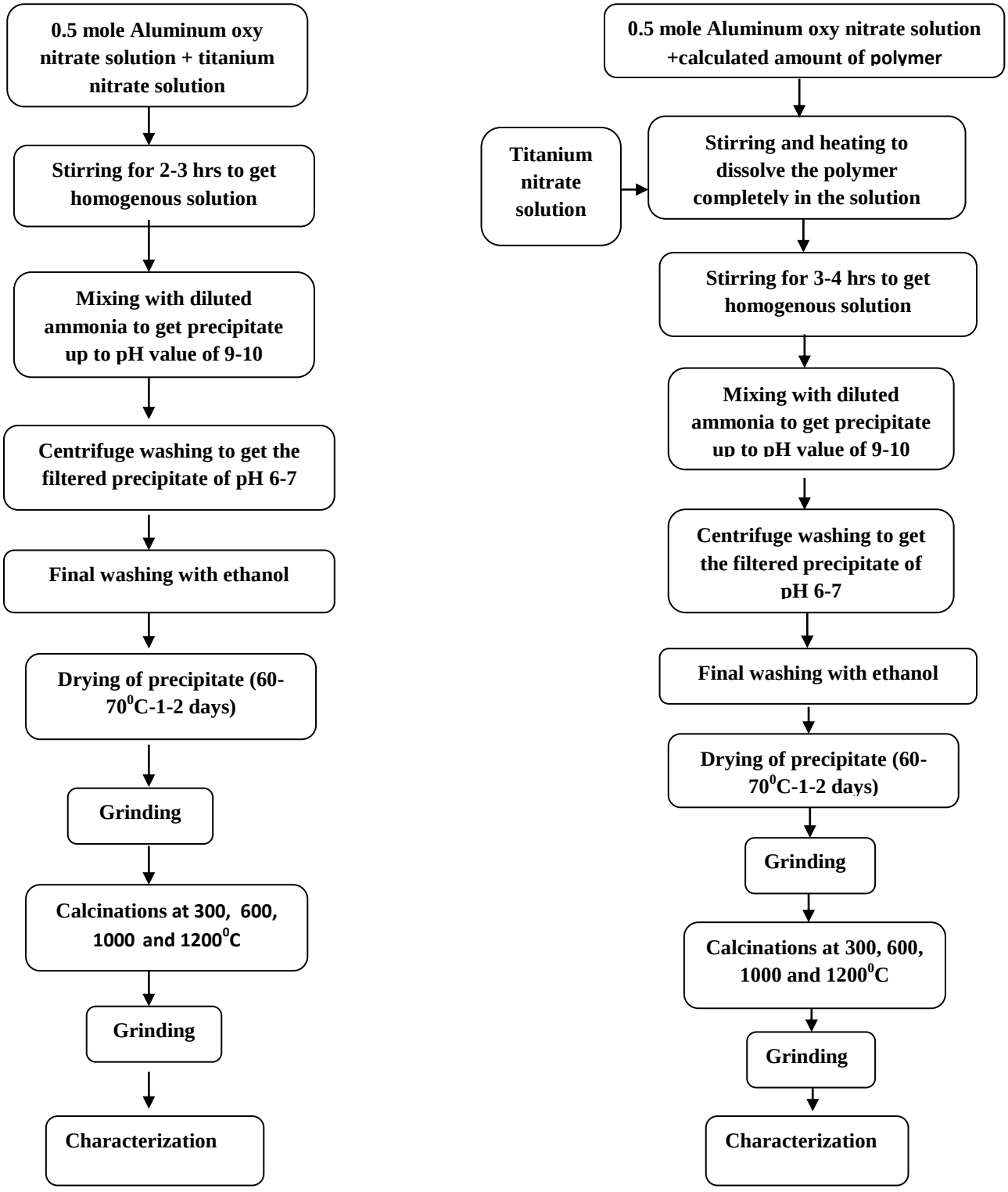

Fig. 5: Flow diagram of 1. Simple co-precipitation route 2. Polymer assisted co-precipitation route

3.4 EXPERIMENTAL INSTRUMENTS:

3.4.1 DIFFERENTIAL SCANNING CALORIMETRY

Thermo-analytical technique includes Differential scanning calorimetry which gives the information about glass transition temperature and melting temperature of given sample with the help of DSC curve. The study of oxidation and other chemical reactions as well as fusion and crystallization study is possible by using this technique.. It works on the priciple that when a sample undergoes any physical transformation like phase transformation, heat will be required by the given sample to maintain the temperature similarity with reference material and it will depend upon the nature of the reaction whether it is endo or exothermic reaction. Taking an example- solid sample while melting into liquid form will require more heat flowing to the sample because it will increase its temperature at the as same rate as that of the reference due to the absorption of heat by the sample. This is endothermic phase transition from solid to liquid. less heat will be required to raise the sample temperature if the sample undergoes any exothermic reaction, such as crystallisation. In this experimental work , we have taken the mass of solder 15mg , temprature range 25 ^{o}C to 300 ^{o}C and rate of temperature changes 10 ^{o}C per minute.

3.4.2 X-RAY DIFFRACTION STUDIES

X-Ray Diffraction machine is a very useful device to characterise materials for the following information such as phase analysis (elemental phase/ inter-metallic phase/ crystalline phase/ non-crystalline phase) , lattice parameter determination, strain determination, texture and orientation analysis, order- disorder transformation. A phillips Pan analytical PW3040/00 X-ray diffractometer was used to characterise the samples prepared by simple co-precipitation and polymer assisted co-precipitation. The scanning range of 2θ was from 15° to 80° with a scanning

speed of 20° min^{-1} and accelerating voltage of 30 KV. The peak was analysed by using X-pert high score software to identify different types of phases.

3.4.3 DILATOMETRY:

Dilatometry is a technique known as thermo analytical used to the measure the shrinkage and expansion of given material under controlled temperature and time.

This is a standardized method which operates on the bases as DIN EN 821, DIN 51045, ASTM E 831 and ASTM E 228. Samples like powders, solid samples, pastes and liquids can be tested by using special type of containers.

Information by DIL Measurement: Following informations can be achieved.

- Determination of the coefficient of thermal expansion (CTE)
- Linear thermal expansion
- Volumetric expansion
- Sintering temperature and sintering step
- Density change
- Determination of glass transition temperature
- Softening points
- Phase transitions
- Influence of additives and raw materials
- Optimizing of firing processes
- Kinetic studies
- Rate-controlled sintering (RCS)

, A pushrod is connected to LVDT system , and on the other, it is in close contact with a sample to measure the length change occurred in given sample during heating and cooling. The anterior part & sample holder are in the same temperature program equal to sample, they will also show expansion. Finally, the total change in length of the sample, pushrod and sample holder will occur. The raw dilatometer data should be correct to get the exact sample behavior. Two methods can be used 1. by using tabulated expansion data for the sample holder material and 2.by using a correction curve. The second method is more useful.

.

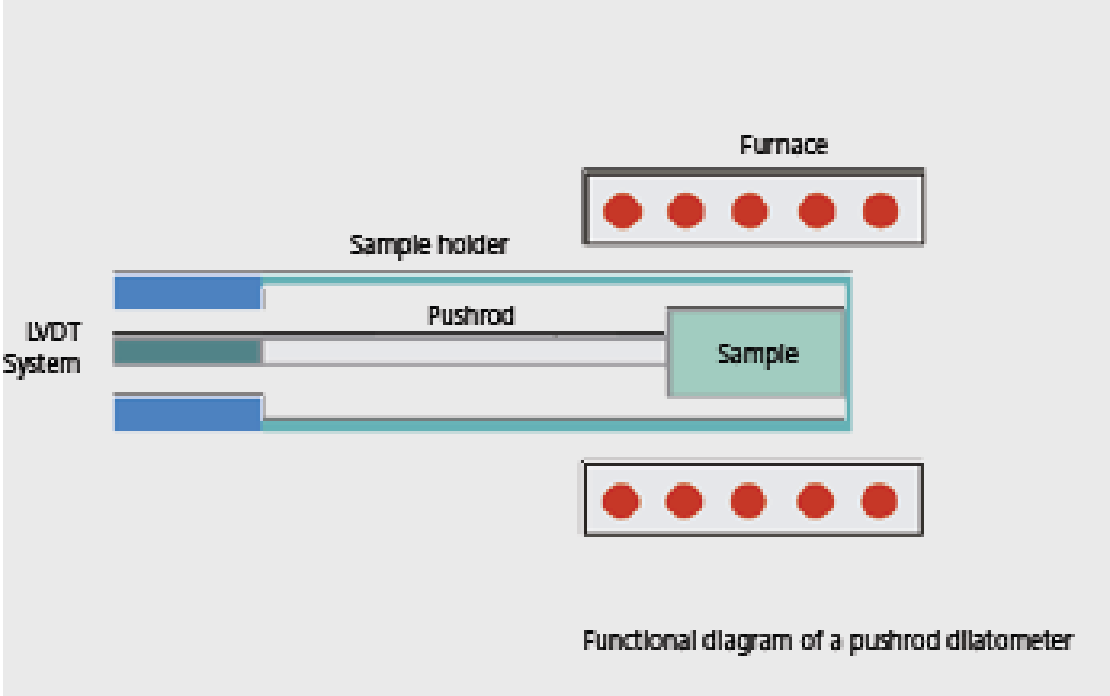

Fig. 6: Dilatromerty instrument for the measurement of shrinkage

3.4.4 FOURIER TRANSFORMATION INFRARED SPECTROPHOTOMETER:

The Fourier Transformation Infrared spectrophotometer measures an infrared spectrum by Fourier-transform of an interferogram. An FTIR uses one of several optical systems; the IRPrestige-21 relies on a Michelson interferometer (Fig. 7). After passing through the aperture, light is turned into a parallel beam by the collimator mirror and enters the beam splitter. A germanium film, deposited on a potassium bromide substrate via evaporation, comprises the beam splitter; it splits the single beam into two, reflecting one to the fixed mirror and transmitting the other to the moving mirror. Both mirrors reflect their beams back to the beam splitter; part of each returning beam is reflected and transmitted. The transmitted light from the fixed mirror and the reflected light from the moving mirror recombine and interfere with each other as they travel towards the collecting mirror. The interference is either constructive or destructive.

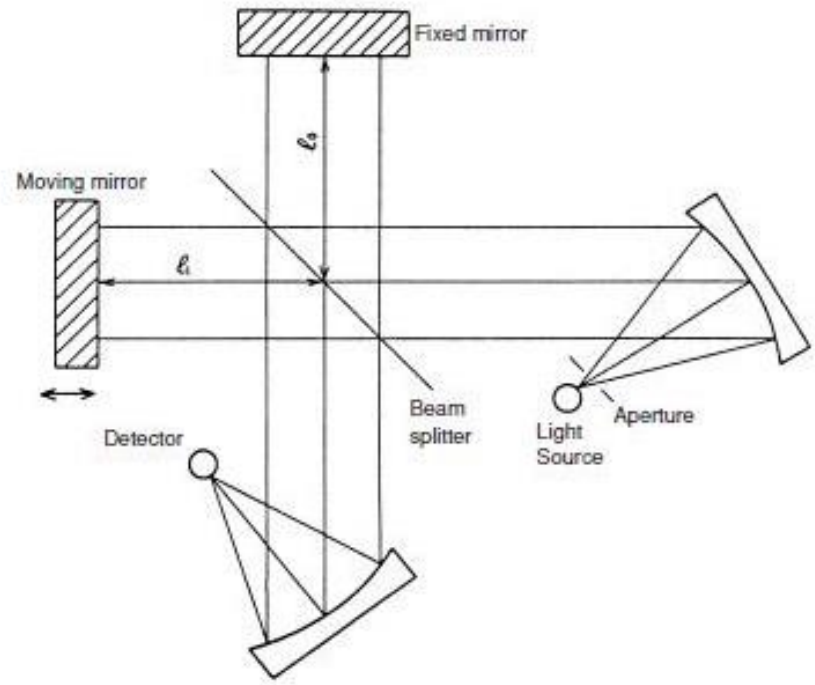

Fig. 7: Michelson interferometer

The three FTIR advantages extend many benefits:

1. Higher sensitivity measurement

2. Measures samples with low transmittance, a small sample size, or a thin layer of film on its surface.

3. Higher speed measurement

4. Higher wave number accuracy

5. Highly accurate spectrum subtraction

3.4.5 FIELD EMISSION SCANNING ELECTRON MICROSCOPE

The scanning electron microscope is a type of electron microscope in which high energy beam of electrons are directed at the specimen. It is used to produce two dimensional image of a specimen of any size and thickness. The electrons produced by the hot filament are accelerated by electric and magnetic fields thus interacting with the sample and producing signals which contain information about the surface or near surface topography, composition and other properties such as electrical conductivity. SEM is primarily used to study the structure of bulk specimens. It can produce very high resolution images of sample surface and give information about less than 1nm in size. The magnification range of conventional SEM is 10x – 200,000x with spatial resolution of 50 – 100 nm can scan areas which vary from 1cm to 5 μm in width. The types of signals produced by a SEM include secondary electrons; back scattered electrons, characteristic X-ray, light (cathodoluminescence). The mode used in SEM micrographs is secondary electron imaging.

SEM has following components

- Electron Gun
- Condenser and Objective lens
- Scan Coil
- Aperture
- Detectors and Display/Date Output devices

  In the present work the solder samples work mechanically polish using standard metallography techniques before the examination. The micrographs of the sample were obtained. The mode used in SEM micrograph is secondary electron imaging.

DENSITY MEASUREMENT

Geometrical density can be easily measured by getting the weight and volume of the samples by using the formula:

● **Geometrical Density = Weight/Volume**

Where volume of pellet = $\pi r^2 h$

Whereas, apparent porosity can be find out by using formula:

● **Bulk Density = D/(W-S)**

● **Apparent porosity A.P.(%) = [(W-D)/(W-S)] x 100**

Where W= soaked weight,

Chapter 4

RESULTS & DISCUSSION

4.1 DSC & TG ANALYSIS

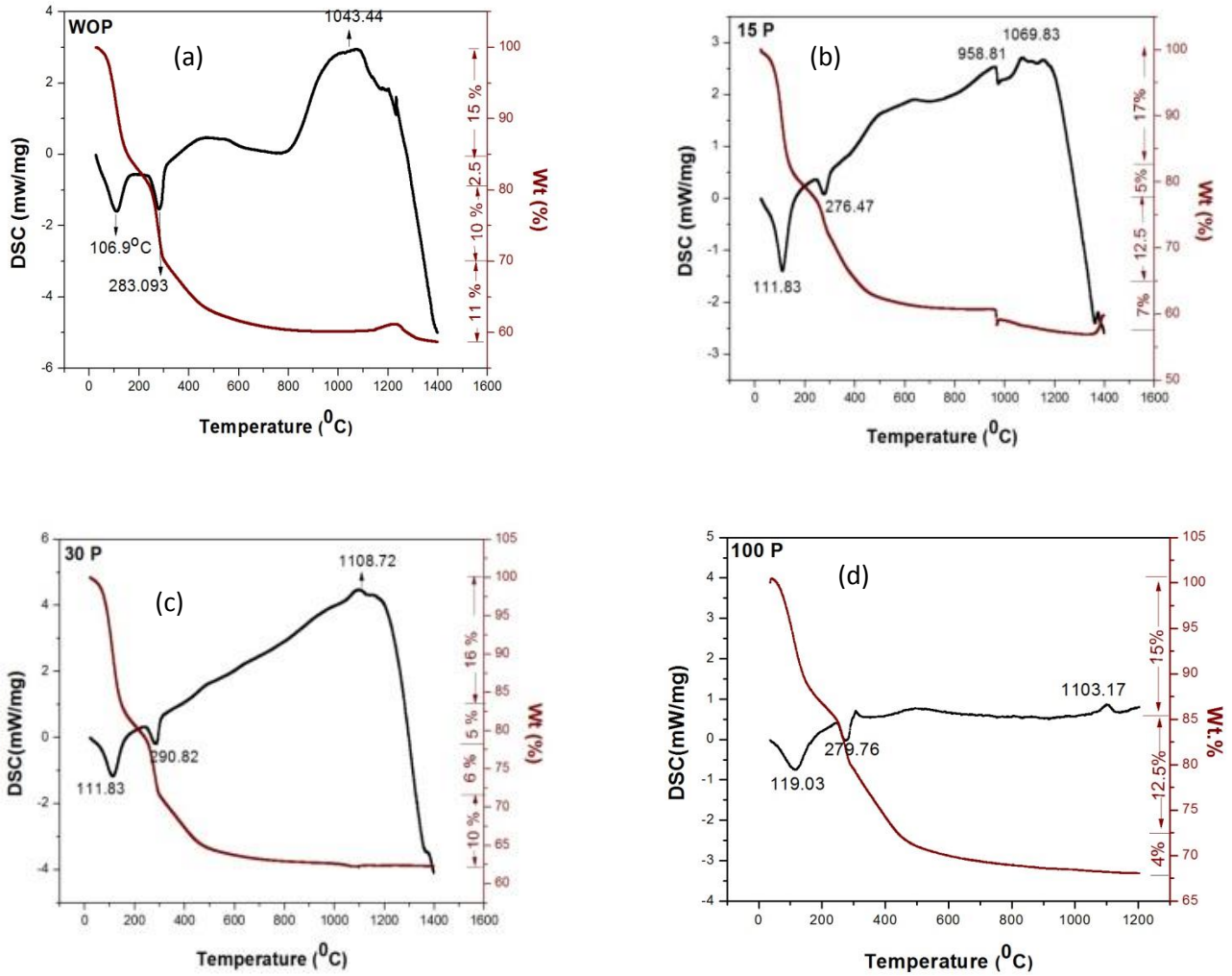

Fig. 8: DSC-TG plots for the Al2O3–13 wt% TiO2 dried composite powder prepared in different polymer concentration (a) without polymer (b) 15 wt. % P123 (c) 30 wt. % P123 (d) 100 wt. % P123

Fig. 8 shows the DSC-TG plots for the Al_2O_3–13 wt. % TiO_2 dried composite powder prepared in different condition. The endothermic peak at 107^oC [Fig. 8(a)] corresponds to the decomposition of physically absorbed water. It is to be mentioned that for polymer added powder similar endothermic peak was observed but peak shifted to 5-10^oC depending on the polymer concentration. Endothermic peak near 280^oC is related to a very early decomposition of gibbsite into γ- alumina [45]. The weight loss in TG plot was around 27 % for samples (WOP, 15P, 30P) and 18 % for sample 100 P upto this temperature range. A broad exothermic peak was observed in the range of 900-1200^oC, that is due to the crystallization of gamma alumina and its transformation in to α- alumina [46]. An endothermic peak at 1300^oC shows the formation of aluminium titanate in the composite precursor [47]. The formation of aluminium titanate was confirmed by the XRD analysis. The low temperature formation of aluminium titanate is attributed to the high area of contact between the fine alumina and titania particles under the present condition where a diffusion rate is favored. It was observed that overall weight loss upto 1400^oC was around 40%. It is to be noted that beyond 600^oC there is negligible weight loss observed. From the DSC-TG analysis we can conclude that the polymer content has little influence on the formation temperature of aluminium titanate in the composite.

Table 4: List of DSC peaks and weight loss analyzed at different temperature ranges

Temperature range	Weight loss
a). WOP	
Up to 106.9°C	15 %
106.9-284°C	25 %
284-400°C	10 %
400-1400^{0}C	11 %
b). 15P	
Up to 200°C	17%
200-276.47°C	5%
276.47- 400^{0}C	12.5%
400-1400°C	7 %
c). 30P	
Up to 200°C	16%
200-290.82°C	5%
290.82- 320°C	6%
320-1400°C	10%
d). 100P	
Upto 200°C	15%
200- 500°C	12.5%
500-1400°C	4%

Temperature	Type of peak
a). WOP	
106.9^0 C	Endothermic peak
283.093^0 C	Endothermic peak
1043.44^0 C	Exothermic peak
1201.34^0 C	Exothermic peak
b). 15P	
111.83°C	Endothermic peak
276.47°C	Endothermic peak
958.81°C	Exothermic peak
1069.83	Exothermic peak
c). 30P	
111.83	Endothermic peak
290.82	Exothermic peak
1108.72	Exothermic peak
d). 100P	
119.73	Endothermic peak
279.76	Endothermic peak
1103.1	Exothermic peak

4.2 X-RAY DIFFRACTION ANALYSIS

XRD analysis was used to identify different phases in the composite powders [Fig. 9(a)-(d)] calcined at 300^{o}C/6h, 600^{o}C/6h, 1000^{o}C/4h, 1200^{o}C/4h, respectively. The powder calcined at 300^{o}C and 600^{o}C shows broad peak and can be matched with γ-alumina. Sarkar et al. also got similar low temperature γ-alumina phase formation [48]. The result was matching with the DSC-TG observation. The powder calcined at 1000^{o}C shows well crystalline peak and the presence of major phase of α- alumina and rutile. Significant concentration of θ-alumina is also present. So, during calcination at 1000^{o}C, γ-alumina was converts to α- alumina and θ-alumina. Kharas et al also got similar θ-alumina phase at high temperature [49]. That may be due to presence of other oxide (Ti-hydroxide) in precipitates. The powder calcined at 1200^{o}C shows well crystalline peak and the presence of only of α- alumina and rutile. No aluminium titanate was formed at 1200^{o}C. Fig.10 shows the XRD pattern of sintered (1650^{o}C/4h) ground pellet. It was observed that there is only Al_2O_3 and Al_2TiO_5 (AT) phase is present. A small amount of TiO_2 phase is present. That means, TiO_2 is reacting with Al_2O_3 and forming AT phase and it is stable at room temperature. It is to be mentioned that with increase in polymer content, percentage of AT phase is enhanced which is maximum at 30P concentration. Fig.11 shows the XRD pattern of 1500^{o}C sintered sample. Significant amount of Al_2TiO_5 phase formed but small amount of TiO_2 retained.

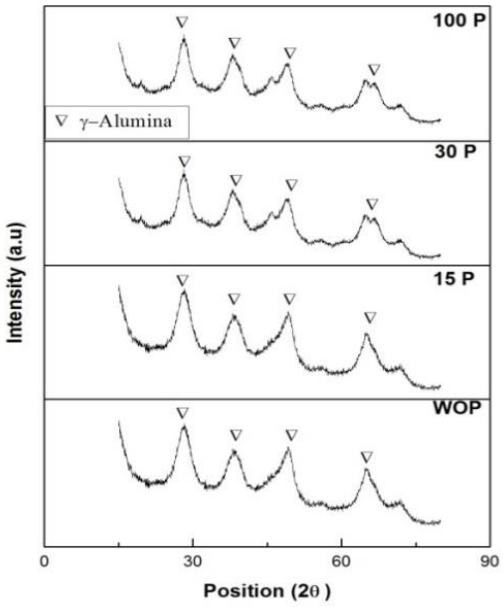

Fig. 9(a): XRD pattern of powder samples calcined at 300^0C

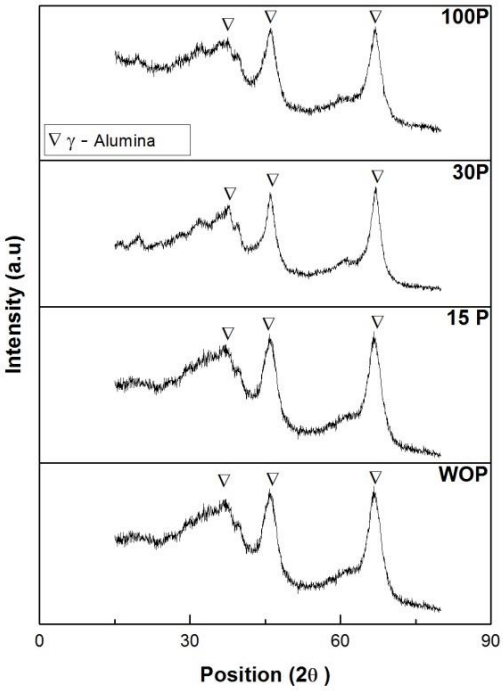

Fig. 9(b): XRD pattern of powder samples calcined at 600^0C

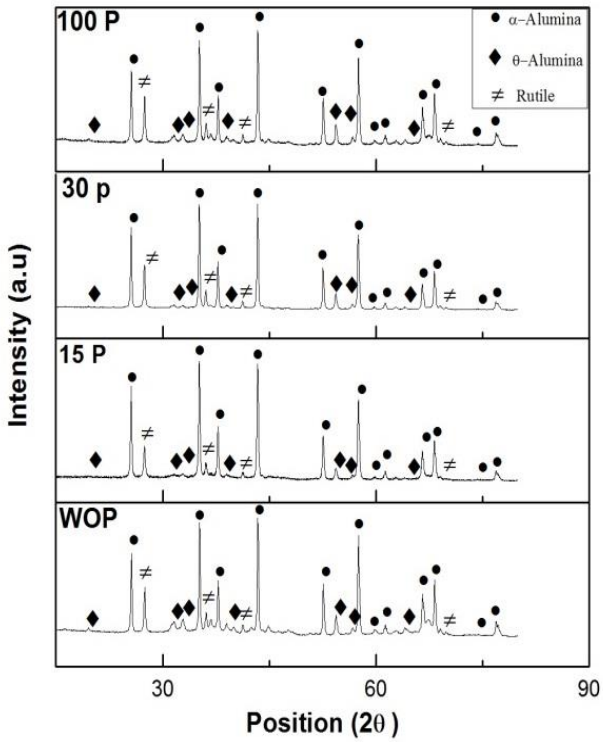

Fig. 9(c): XRD pattern of powder samples calcined at 1000^0C

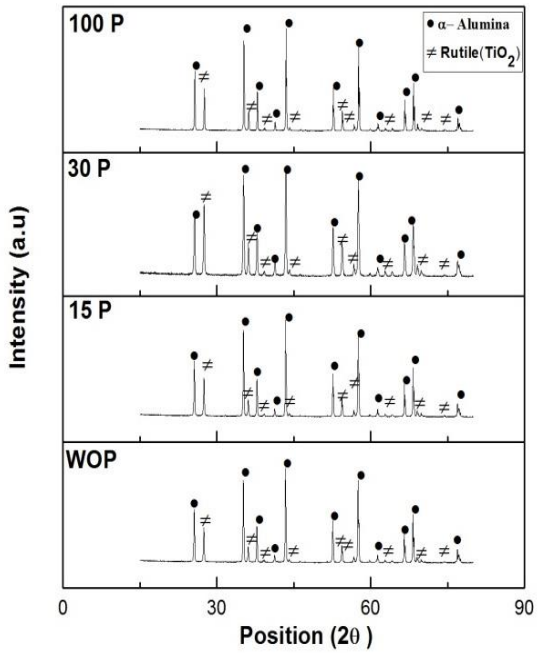

Fig. 9(d): XRD pattern of powder samples calcined at 1200^0C

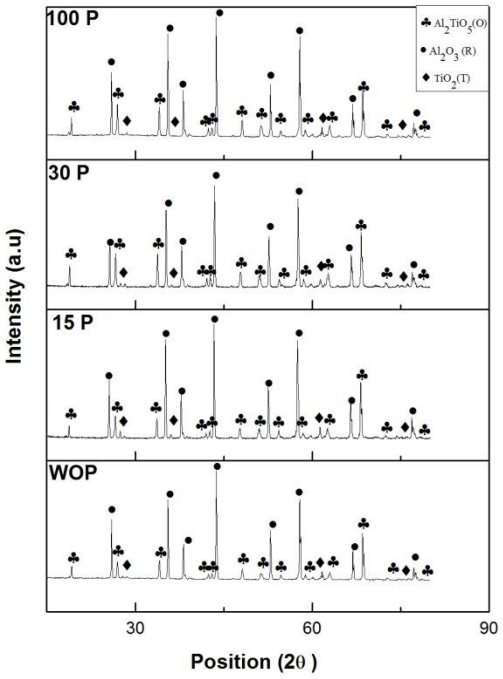

Fig. 10: XRD pattern of pellets sintered at 1650^0C

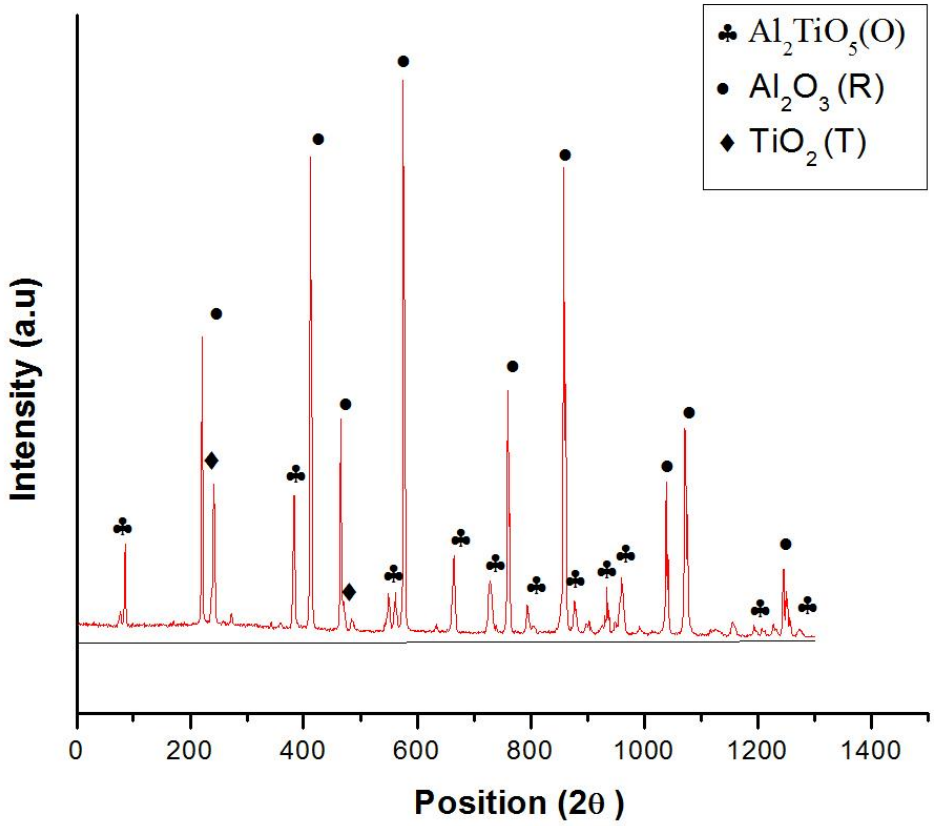

Fig. 11: XRD pattern of pellet sintered at 1500^0C

4.3 SHRINKAGE BEHAVIOUR OF AL_2O_3–13 wt. % TIO_2 COMPOSITE

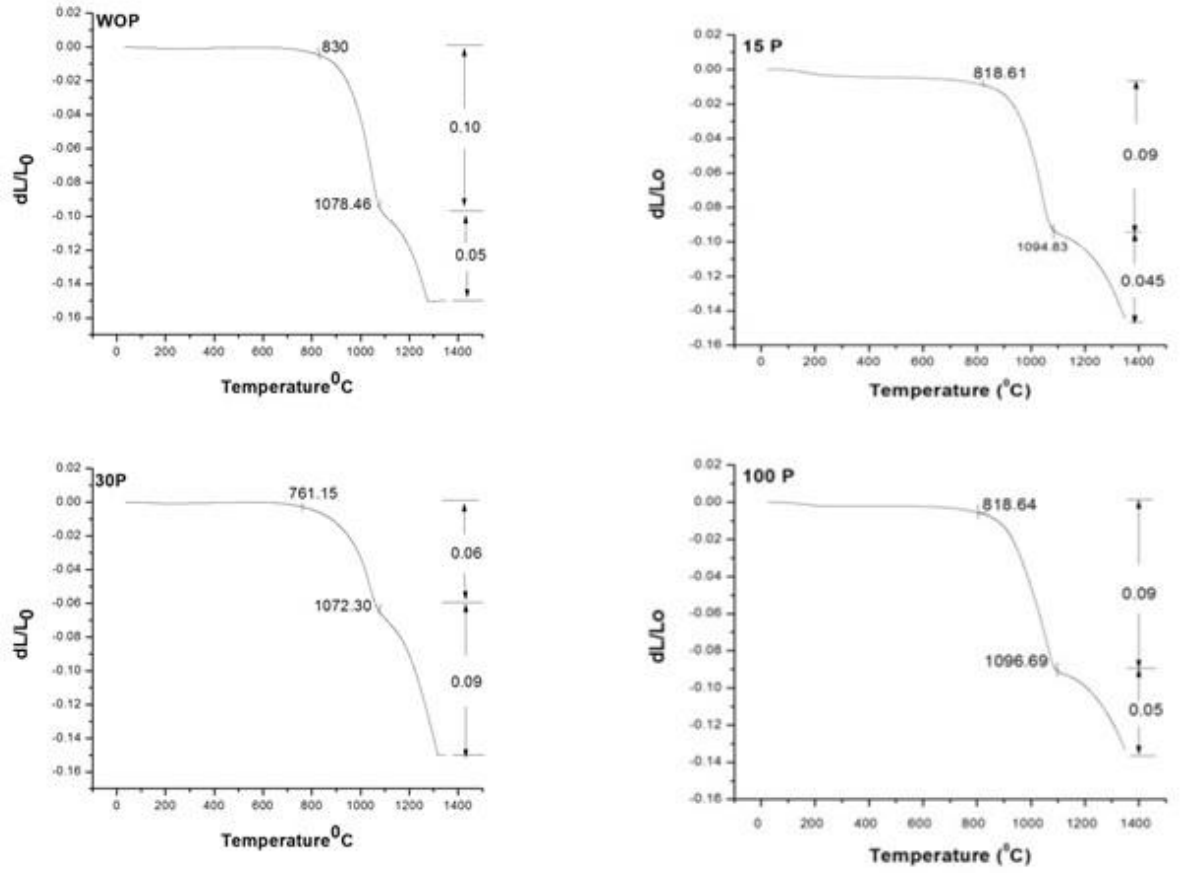

Fig.12: Shrinkage behavior of composite powder calcined at 600°C with different polymer concentration (a) without polymer (b) 15 wt. % P123 (c) 30 wt. % P123 (d) 100 wt. % P123

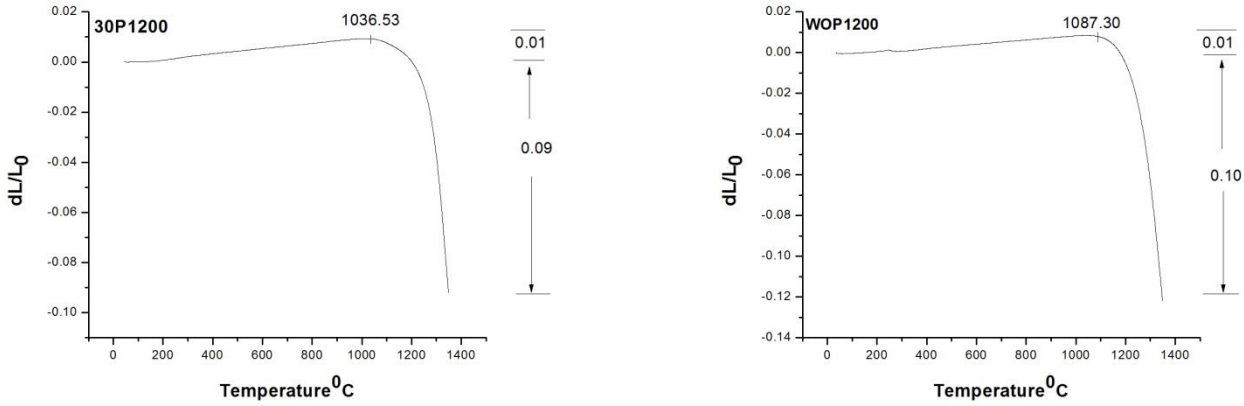

Fig.13: Shrinkage behaviour of composite powder calcined at 1200°C with different polymer concentration (a) 30 wt. % P123 (b) without polymer

The shrinkage behaviour of Al_2O_3–13 wt% TiO_2 composite was studied using 600^oC/6h calcined powder. Fig.12 (a)-(d) shows shrinkage behavior of powder compact of without polymer and polymer (P123) added co-precipitated sample. It was observed that the shrinkage starting above 800^oC for all the samples except 30P powder. For 30P sample shrinkage starts around 762^oC. The shrinkage observed at low temperature is due to the fine particle size and highly reactive nature of the powder. Jayasankar et al. [30] prepared Al_2O_3-20 wt. % TiO_2 by sol-gel route. In their case shrinkage starts above 1100^oC. The total linear shrinkage of the sample was about 13-15 %. In all the samples prepared by co precipitation, there is a change in the slope of shrinkage vs temperature plot near 1100^oC, which may be due to bimodal distribution of particle size in the powder or the crystallization of γ-alumina in to α- alumina. The evidence of the crystallization of γ-alumina in to α- alumina is observed in the DSC-TG graph. To understand the sintering behavior, co-precipitated powder was calcined at 1200^oC and shrinkage behavior was studied. It was observed that change in the slope of shrinkage vs temperature plot around 1100^oC is absent in this case. So, it was confirmed that slope change in earlier case was due to crystallization of γ-alumina to α- alumina. Now the total shrinkage was 10% which is less than the earlier case. That may be due to reduction in reactivity of the powder with increase in calcination temperature. It is to be noted that the onset temperature for WOP and 30P samples were 1087^oC and 1036^oC, respectively. The lower onset temperature for polymer added sample is due to smaller particle size of the latter.

4.4 FTIR ANALYSIS

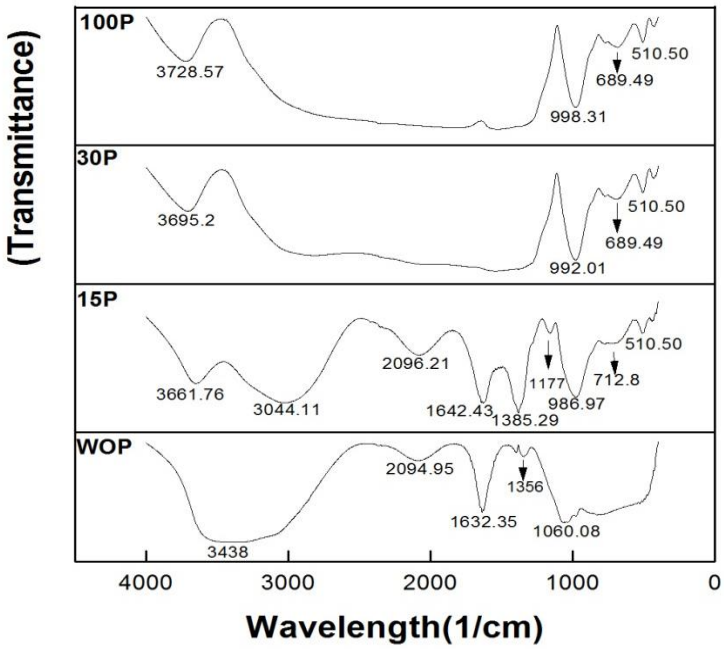

Fig. 14: FTIR analysis of the dried samples prepared by simple co-precipitation and polymer assisted co-precipitation route (a) without polymer (b) 15 wt. % P123 (c) 30 wt. % P123 (d) 100 wt. % P123

To find out the changes taking place within the powder with the change in polymer type concentration, it is important to consider the spectral ranges (i) 3000-3500 cm^{-1} representing OH stretching vibrations of water and OH groups appear and (ii) 200-850 cm^{-1} for Al-O and Ti-O stretching and bending vibrations .

Figure 14 shows the FTIR spectra of the different samples of Al_2O_3–13 wt. % TiO_2 powders prepared by simple co precipitation and polymer assisted co-precipitation route having different concentration of polymer in the range of wave number 400 and 4500 cm^{-1}. The dried powder of Al_2O_3–13 wt. % TiO_2 precursor powder having spectrum clearly shows broad absorption around 3300 - 3700 cm^{-1}. This is attributed to the hydroxyl groups (O–H) stretching vibration [50, 51]. The corresponding bending mode appears as medium intense band near around 1060 cm^{-1}.

In the region 500-750 cm^{-1}, octahedral Al-O coordination gives Al-O stretching modes and in the region 330-450 cm^{-1}, it gives bending modes [52-54]. Whereas tetrahedral coordination is expected to give the Al-O stretching modes in the narrow region 750-850cm^{-1} and bending modes between 250 and 300cm^{-1} [52-54]. Vibrational frequencies of Ti-O, are overlapped with Al-O, it can be easily concluded the from the IR curve that the IR active Ti-O stretching modes appear below 730cm^{-1} [55,56]. Hence, frequencies appearing above 750cm^{-1} can only be due to Al-O stretching modes with tetrahedral coordination.

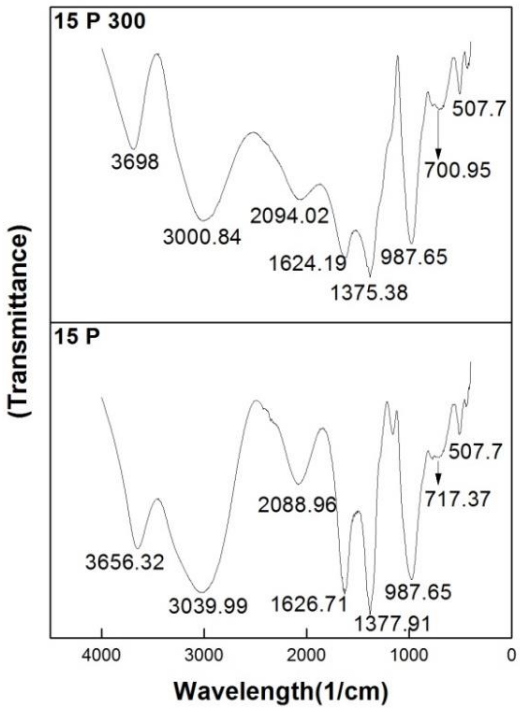

Fig 15: Comparison of dried and calcined (300°C) sample having 15% P123

The broad peak near the range 3,650 cm^{-1} remains in the calcined powders which are attributed to the adsorbed water in air. We calcined the powder sample of 30P to investigate to compare the difference in IR curve. There is not much difference in the peak values. Only the intensity of peaks are reduced which is showing the formation of compound with increasing temperature. The formation of Al_2O_3 and TiO_2 with increasing temperature is also evidenced by other papers.

4.6 FESEM ANALYSIS

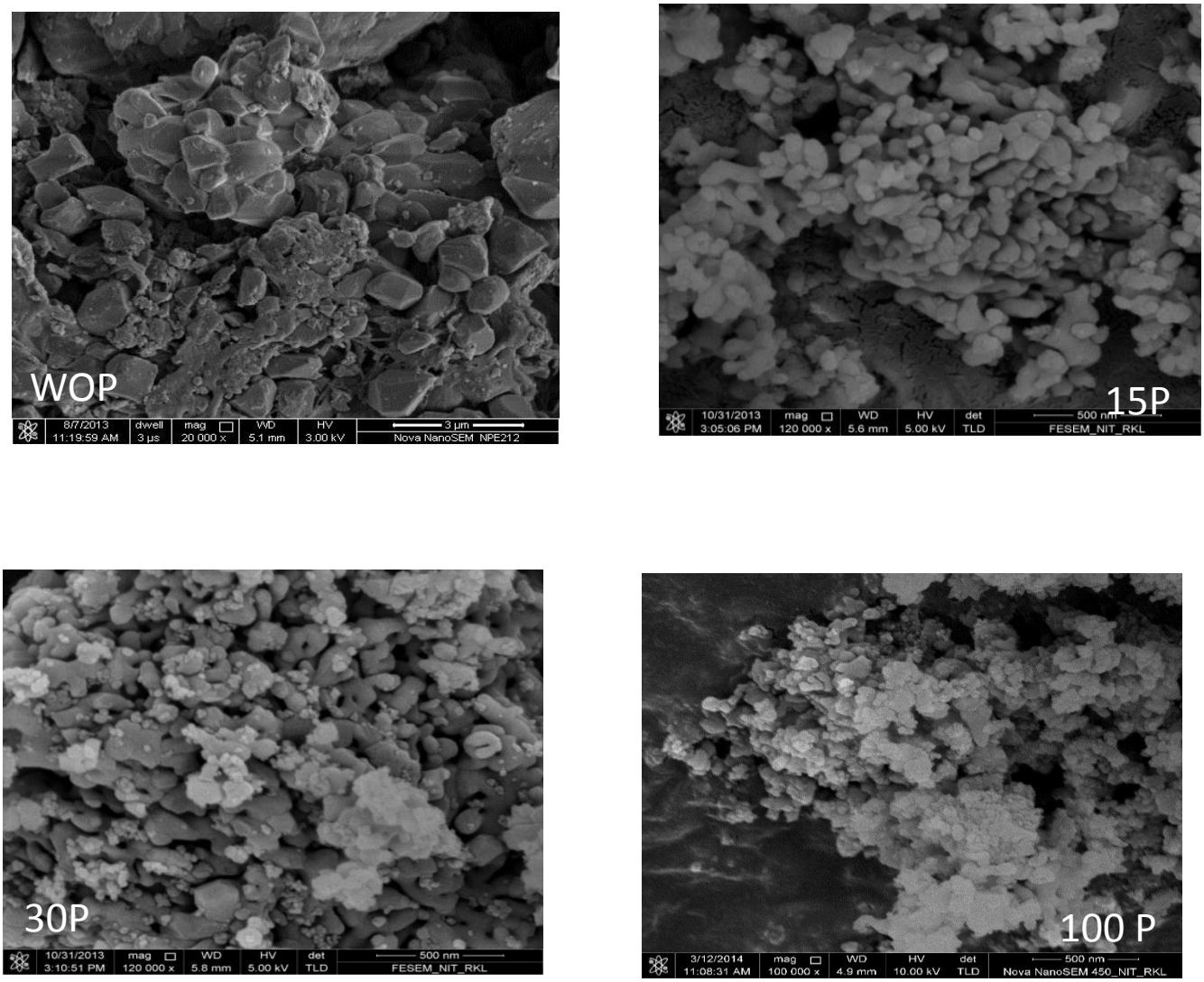

Fig.16: FESEM micrograph of the dried samples prepared by simple co-precipitation and polymer assisted co-precipitation route (a) without polymer (b) 15 wt. % P123 (c) 30 wt. % P123 (d) 100 wt. % P123

In the FESEM micrograph of WOP sample [Fig.16 (a)], particle size in the range of 0.786-2.12 μm has been observed. On addition of polymer, to the base sample in 15, 30 and 100 wt%, decrease in the particle size has been observed. Particle size was in the range of 61-173nm, 41-138nm and 35-80 nm has been observed in the FESEM micrograph [Fig.16 (b, c and d)] for samples 15P, 30P, and 100P respectively. The morphology has improved with increasing the polymer content. The well-defined boundary of the rounded grains is achieved.

Table 5: Particle size range determined by FESEM analysis

Sample name	Particle size range
WOP	0.786- 2.128 μm
15 P	61-173 nm
30 P	41-138 nm
100 P	35-80 nm

4.7 STUDY OF SINTERING BEHAVIOUR

Table 6: Density and volume shrinkage of samples sintered at 1650°C

SAMPLE NAME	SINTERING RATE	GEOMETRICAL DENSITY	TRUE DENSITY	RELATIVE DENSITY	VOLUME SHRINKAGE
1.	1650^0C	3.80	3.96	95.9%	49.25%
2.	1650^0C	3.72	3.96	94%	48.88%
3.	1650^0C	3.80	3.95	96%	50%
4.	1650^0C	3.70	3.95	93.6%	45.18%

4.7.1 DENSITY MEASUREMENT:

It is to be noted that no significant change in density was observed for polymer added sample compared to without polymer added one. The change in density is also examined with the change in sintering temperature .when we decreased the sintering temperature from 1650°C to 1500°C, the decrease in density is observed.

4.8 FESEM ANALYSIS OF SINTERED PELLETS:

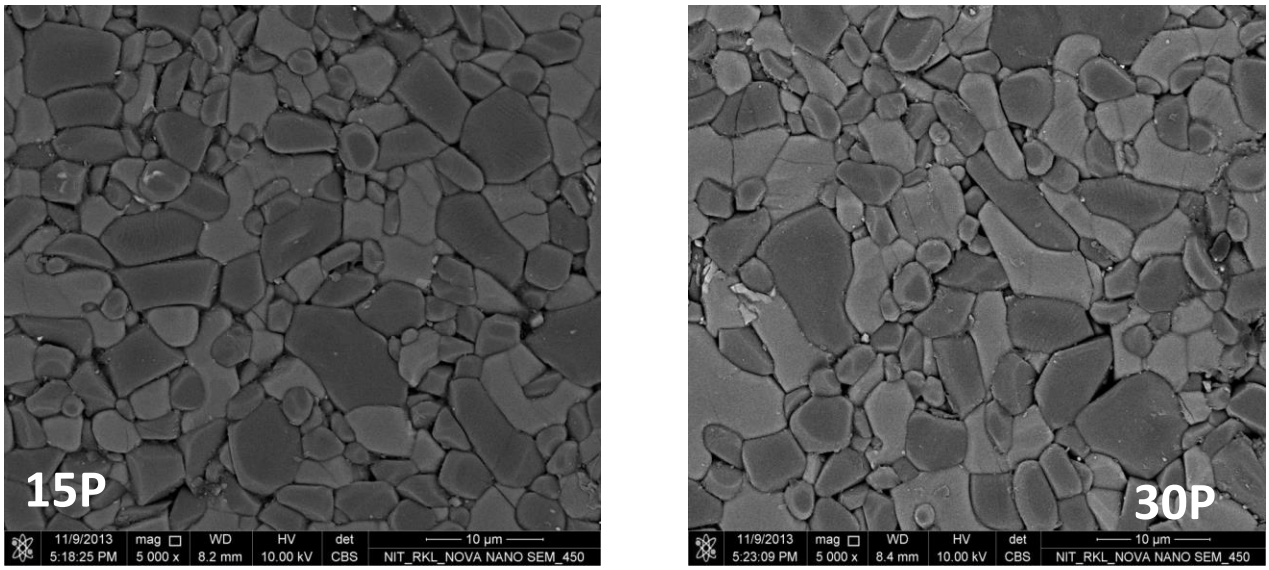

Fig 17: FESEM micro pictograph of pellets sintered at 1650^0C (a) 15P; (b) 30 P

The microstructures of the sintered samples were analyzed by using Field Emission Scanning Electron Microscope. Two samples were examined having 15% and 30% polymer P123 content which is shown in the figure. Figure is showing that highly dense structure was achieved by this polymer assisted route which is higher compared to the density achieved by solid state route of the same composition [57]. The darker grains are alumina and lighter grains are Al_2TiO_5. Microstructure shows homogeneous distribution of the two phase.

Chapter 5

CONCLUSION

&

FUTURE WORK

An alumina-titania composite powder containing 13 wt. % titania was prepared by polymer assisted co-precipitation technique. Co-polymer Pluronic P-123 (0, 5, 15, 30, and 100 wt. % of the composite powder) was used in the precipitation process. The effect of polymer addition on phase formation, morphology and size of the composite powder, densification, microstructure and mechanical properties of the composite was studied. Summary of the results given below

- From XRD and DSC-TG analysis it was observed that around 300^{o}C γ-alumina but no trace of rutile/anatase was observed upto 1000^{o}C. Beyond 900^{o}C γ-alumina transform to α and θ alumina. At 1200^{o}C calcined powder only α–alumina and rutile phase is observed. Formation of Al_2TiO_5 was not visible. From the DSC-TG analysis we can conclude that the polymer content has little influence on the formation temperature of aluminium titanate in the composite.
- It was observed that polymer addition during precipitation significantly reduces the particle size. With polymer addition particle size decreased to 35-80 nm range in calcined (1200^{o}C) powder. FESEM- EDAX analysis shows a homogeneous distribution of alumina-titania phase. FTIR analysis of uncalcined dried powder shows no presence of polymer in washed dried product.
- Shrinkage behavior of 600^{o}C calcined nanocomposite powder shows overall linear shrinkage of 15% upto 1400^{o}C. It consists of two step shrinkage. Slope change in linear shrinkage vs temperature plot around 1100^{o}C due to γ - θ to α alumina phase transition as 1200^{o}C calcined powder this slope change is absent. Polymer added precipitated sample has better sinterability as shrinkage starts around 1035^{o}C. The lower onset temperature for polymer added sample is due to smaller particle size of the latter.
- Al_2O_3-TiO_2 nanocomposite powder can be sintered to more than 95% of relative density achieved at 1650^{o}C. Phase analysis of sintered sample shows formation of Al_2TiO_5 phase. With increase in polymer content, percentage of Al_2TiO_5 phase is enhanced which is maximum at 30P concentration. The low temperature formation of aluminium titanate is attributed to the high area of contact between the fine alumina and titania particles under the present condition where a diffusion rate is favoured.
- FESEM analysis of sintered pellet shows uniform distribution of Al_2O_3 and Al_2TiO_5 phase.

FUTURE WORK:

1. Mechanical property of the sintered composite specimen.
2. Same powder preparation should be repeated with a homo polymer (eg. PEG)
3. It will be interesting to study whether this simple process can be utilized for high concentration of TiO_2 concentration (eg. 20, 40, 50 wt.%).

REFERENCES

1. Wan et al, Preparation of Nanocomposites of Alumina and Titania, US Patent 7,217,386 B2, May 15, 2007.
2. N.P. Padture, J.L. Runyan, S.J. Bennison, L.M. Braun, B.R. Lawn, Journal of the American Ceramic Society 76, 2241–2247 (1993).
3. Miriam Floristán et al, Fusion Engineering and Design, 86 1847–1850 (2011).
4. D. Goberman, Y.H. Sohn, L. Shaw, E. Jordan, M. Gell, "Microstructure development of Al2O3–13wt.%TiO2 plasma sprayed coatings derived from nanocrystalline powders", Acta Materialia, 50, 1141–1152, (2002).
5. "Alumina (Aluminium Oxide) – The Different Types of Commercially Available Grades" Retrieved 2007-10-27.
6. Y. Teng, Y. Zhuang, G. Lin, J. Zhou, B. Zhu, J. Qiu, J. Alloys Compd. 479, 378–381 (2010).
7. S.E. Kim, J.H. Lim, S.C. Lee, S.-C. Nam, H.-G. Kang, J. Choi, Electrochim. Acta, 53 4846–4851(2008).
8. S. Iftekar, J. Grins, G. Svensson, J. Loof, T. Jarmar, G.A. Botton, C.M. Andrei, H.J. Engqvist, J. Eur. Ceram. Soc. 28 747–756 (2008).
9. S. Kurien, J. Mathew, S. Sebastian, S.N. Potty, K.C. George, Mater. Chem. Phys. 98 470–476 (2006).
10. Paglia, G. (2004). "Determination of the Structure of γ-Alumina using Empirical and First Principles Calculations Combined with Supporting Experiments" Curtin University of Technology, Perth.Retrieved 2009-05-05.
11. Greenwood, Norman N.; Earnshaw, Alan (1984). Chemistry of the Elements Oxford Pergamon Press. pp. 1117–19. ISBN 0-08-022057-6.

12. L. Zhang, A.J. Xie, Y.H. Shen, S.K. Li, J. Alloys Compd. 505, 579–583(2010) .

13. L. Zheng, M. Xu, T. Xu, Sens. Actuators, 66, 28–30 (2000).

14. A. Dodd, A. McKinley, T. Tsuzuki, M. Saunders, J. Alloys Compd. 489, L17–L21(2010).

15. "Market Study: Titanium Dioxide" Ceresana.Retrieved, 21 May 2013.

16. H.K. Mishra, M. Stanciulescu, J.-P.Charland, J.F. Kelly, Appl. Surf. Sci., 254, 7098–7103 (2008).

17. J. Choi, J. Kim, J.S. Yoo, T.G. Lee, Powder Technol., 181, 83–88 (2008).

18. T.M. Zima, N.I. Baklanova, N.Z. Lyakhov, Inorg. Mater.44, 146 (2008).

19. F. Vaudry, S. Khodabandeh, M.E. Davis, Chem. Mater. 8, 1451–1464 (1996).

20. V.R. Gonzalez, R. Zanella, G. de Angel, R. Gomeza, J. Mol. Catal. 281, 93–98 (2008).

21. T. Korim, I. Kotsis, Effects of additives on the properties of Al2TiO5 ceramics, Mater. Sci. Forum, 414–415, 117–120 (2003).

22. V. Buscaglia, P.Nanni, M. Leoni, Thermodynamics and kinetics of decomposition of Al2TiO5-base ceramics, Key Eng. Mater., 132–136, 810–813 (1997).

23. M. Zaharescu, M. Crison, D. Crison, N. Drãgan, A. Jitianu, M. Preda, Al2TiO5 proportion starting with reactive powders obtained by sol–gel method, J. Eur.Ceram. Soc., 18, 1257–1264 (1998).

24. P. Olkonomou, Ch. Dedloudis, C.J. Stournaras, Ch. Ftiose, Stabilized tialite–mullite composites with low thermal expansion and high strength for catalytic converters, J. Eur. Ceram. Soc., 27, 3475–3482 (2007).

25. L. Stonciu, J.R. Groza, L. Stoica, C.P. Lapcianu, Influence of powder precursors on reaction sintering of Al2TiO5, Scripta Mater., 50, 1259–1262 (2004).

26. B. Freudenberg, A. Mocellin, Aluminum titanate formation by solid-state reaction of fine Al2O3 and TiO2 powders, J. Am. Ceram. Soc., 70 (1), 33–38 (1987).
27. SerkanAball ”Effect of TiO2 doping on microstructural properties of Al2O3-based single crystal Ceramics” Journal of Ceramic Processing Research. Vol. 12, No. 1, pp. 21~25 (2011).
28. Sh.Mohseni Meybodi et al., Ceramics International, 39, 977–982 (2013).
29. A. Borrell et al., Composites, Part B 47, 255–259 (2013).
30. M. Jayasankar et al., Materials Chemistry and Physics, 124, 92–96 (2010).
31. Heromichi Okamura, Eric A. Barringer, H. Kent Bowen, Volume 69, Issue 2, pages C-22–C-24, February 1986.
32. C.G. Li et al.,Journal of Alloys and Compounds, 576, 187–194 (2013).
33. S.-W.Leeetal. MaterialsLetters, 107, 10–13 (2013).
34. M. Dashliborun et al., Chemical Engineering Journal, 226, 59–67 (2013).
35. U.O. Akkaya Arıer, F.Z. Tepehan, Composites, Part B 58, 147–151 (2014).
36. Hiromichi Okamura et.al., Journal Of Materials Science 24, 1867-1880 (1989)
37. Patnaik, P. Dean's Analytical Chemistry Handbook, 2nd ed. McGraw-Hill, 2004.
38. N. M. Bobkova, I. V. Kavrus, E. V. Radion and N. F. Popovskaya; Glass and Ceramics, Vol-55, No. 5-6 (1998).
39. T. Hernandez, M. C. Bautista CIEMAT, Avenida Complutense, 22, 28040, (2004).
40. José Ortiz-Landeros, Carlos Gómez-Yáñez, Rigoberto López-Juárez, Journal of Advanced Ceramics, 1(3), 204-220 (2012).
41. Yu-Tzu Huang, Masataka Imura, Yoshihiro Nemoto, Sci. Technol. Adv. Mater., 12, 045005 (6pp) (2011).

42. Zeinab Mosayebi, Mehran Rezaei, Narges Hadian, Fazlollah Zareie Kordshuli, Fereshteh Meshkani, Materials Research Bulletin, 47, 2154–2160 (2012).

43. Rongrong Jiang, Tao Huang, Jiali Liu, Jihua Zhuang, Aishui Yu, Electrochimica Acta, 54, 3047–3052 (2009).

44. O. L. Galkina, V. V. Vinogradov, A. V. Agafonov and A. V. Vinogradov, International Journal of Inorganic Chemistry, Volume, Article ID 108087, 8 pages (2011).

45. T. Hernandez, M.C. Bautista, Journal of the European Ceramic Society, 25, 663–672 (2005).

46. Dianying Chen Æ Eric H Jordan, J Sol-Gel Sci Technol, 50, 44–47 (2009).

47. M. Jayasankar et al., Materials Chemistry and Physics, 124, 92–96 (2010).

48. D. Sarkar et al. / Composites: Part A 38 (2007) 124–131

49. Kharas et al., Stabilized crystalline alumina compositions US Patent 5877106, 1999

50. Yashima M, Kato T, Kakihana M, Gulgun MA, Matsuo Y, Yoshimura M, Crystallization of hafnia and zirconia during the pyrolysis of acetate gels, J Mater Res 12(10):2575–2583 (1997).

51. Chen DY, Jordan E, Gell M Thermal and crystallization behavior of zirconia precursor used in the solution precursor plasma spray process, J Mater Sci, 42(14),5576–5580 (2007).

52. Ph. Colomban, J. Mater. Sci., 24, 3002 (1989).

53. Paul McMillan and Bernard Piriou, J. Non. Cryst. Solids, 53, 279 (1982).

54. Mazza Daniele, Vallino Mario, and Busea Guide, J. Am. Ceram. Soc., 75, 1929 (1992).

55. M. Ocana, V. Fornes, J. V. Garcia Ramos, and C. J. Serna, J. Solid State Chem. 75, 364 (1988).

56. B. G. Varshai, V. N. Denison, B. N. Mavrin, G. A. Parlova, V. B. Podo Bedov, and Kh. E. Sterin, Opt. Spectrosc, 47, 619 (1979).

57. B.Tech Thesis Snehalata Kumari, NIT Rourkela (2013).